ACS Biomaterials SCIENCE & ENGINEERING

Article

pubs.acs.org/journal/abseba

Bortezomib Increases the Cancer Therapeutic Efficacy of Poly(amino acid)−Doxorubicin

Na Shen,[†] Jian Jiang,[†,‡] Dawei Zhang,[†] Guanyi Wang,[†,§] Shixian Lv,[†] Yanjie Jia,[†] Zhaohui Tang,*[,†] and Xuesi Chen[†]

[†]Key Laboratory of Polymer Ecomaterials, Changchun Institute of Applied Chemistry, Chinese Academy of Sciences, Changchun 130022, P. R. China

[‡]University of Chinese Academy of Sciences, Beijing 100039, P. R. China

[§]Edmond H. Fischer Signal Transduction Laboratory, School of Life Sciences, Jilin University, Changchun 130012, P. R. China

ABSTRACT: Currently, chemotherapy is still a primary method to treat cancers. Doxorubicin is a regular chemotherapy drug, and a previous study indicated that mPEG$_{5k}$-*b*-P(Glu$_{10}$-*r*-Phe$_{10}$)−doxorubicin is a more excellent nanodrug for cancer therapy, as it created a therapeutic advantage compared with free doxorubicin. Therefore, the efficacy of doxorubicin-resistant tumor treatment was investigated in this paper. While the cell viability and cell uptake results did not reflect an advantage of the nanodrug in drug-resistant tumors, comparison of the genetic expression of sensitive and resistant tumor cells highlighted NFκB. The proteasome inhibitor bortezomib, which is approved clinically and may influence the NFκB activity, was thus employed. The MTT assay and flow cytometry indicated that it could increase the therapeutic efficacy of poly(amino acid)−doxorubicin, and Western blot results showed that bortezomib and poly(amino acid)−doxorubicin can synergistically diminish NFκB expression. The synergism was confirmed through the orthotopic xenograft model in vivo. Thus, bortezomib can enhance the cancer therapeutic efficiency of poly(amino acid)−doxorubicin not only during the sensitive period but also during the resistant period. This makes the combination of bortezomib and poly(amino acid)−doxorubicin a potent strategy and guidance for the clinic.

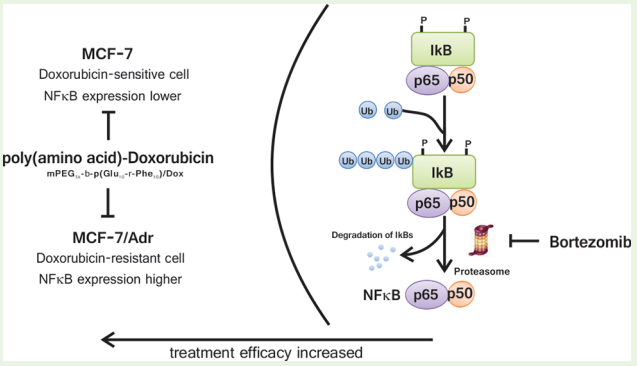

KEYWORDS: *nanodrug, chemotherapy, multidrug resistance, bortezomib, NFκB*

INTRODUCTION

Breast cancer is one of the most critical malignancies and threats to women, and its incidence is rising continuously.[1] Chemotherapy remains the leading treatment strategy for cancer among conventional treatment modalities.[2] The efficacy of routine chemotherapy is significantly hampered by multidrug resistance (MDR) and severe systemic toxicity.[3] In a previous study,[4] an amphiphilic anionic poly(amino acid) copolymer with three functionalized domains, methoxy poly(ethylene glycol)-*b*-poly(L-glutamic acid-*r*-L-phenylalanine) (mPEG$_{5k}$-*b*-P(Glu$_{10}$-*r*-Phe$_{10}$)), was synthesized and used as a nanovehicle for delivery of the cationic anticancer drug doxorubicin hydrochloride (Dox·HCl) via electrostatic interactions for cancer treatment. The poly(amino acid)−doxorubicin (mPEG$_{5k}$-*b*-P(Glu$_{10}$-*r*-Phe$_{10}$)−doxorubicin, n-Dox) had higher cell proliferation inhibition and uptake, with the maximum tolerated dose (MTD) increasing from 5 mg·kg^{-1} for Dox·HCl to 15 mg·kg^{-1} for n-Dox on a Dox·HCl base. Thus, n-DOX demonstrated a significant safety profile and excellent therapeutic efficacy.

One of the advantages of nanodrug is to overcome MDR, which is defined as the resistance of cancer cells to one chemotherapeutic drug, followed by resistance to other chemotherapeutic drugs that may have different structures and action mechanisms.[5] It is estimated that more than 90% of patients that die from cancers are affected by MDR to different extents.[6] A common alteration underlies the membrane of cancer cells, known as the overexpression of drug efflux pumps. Drug efflux pumps are a superfamily of adenosine triphosphate binding cassette (ABC) transporters.[7] On the basis of the above mechanism, the nanodrug was applied to avoid or reduce MDR pump efflux of the drug through lysosome escape.[8] P-glycoprotein (P-gP) siRNA or molecular inhibitor was used to increase the therapeutic efficacy of the multidrug-resistant tumors.

Although the nanodrug and P-gP inhibition treatment succeeded in multidrug-resistant tumors to some extent, MDR remains a major concern, and overcoming the resistance is still a challenge to achieve a better outcome. Efforts of other mechanisms should be considered to attribute to this system. From the molecular biology aspect, the resistant tumor cells exhibit other

Special Issue: Biomaterials Science and Engineering in China

Received: August 31, 2017
Accepted: October 18, 2017
Published: October 18, 2017

DOI: 10.1021/acsbiomaterials.7b00639
ACS Biomater. Sci. Eng. 2018, 4, 2053−2060

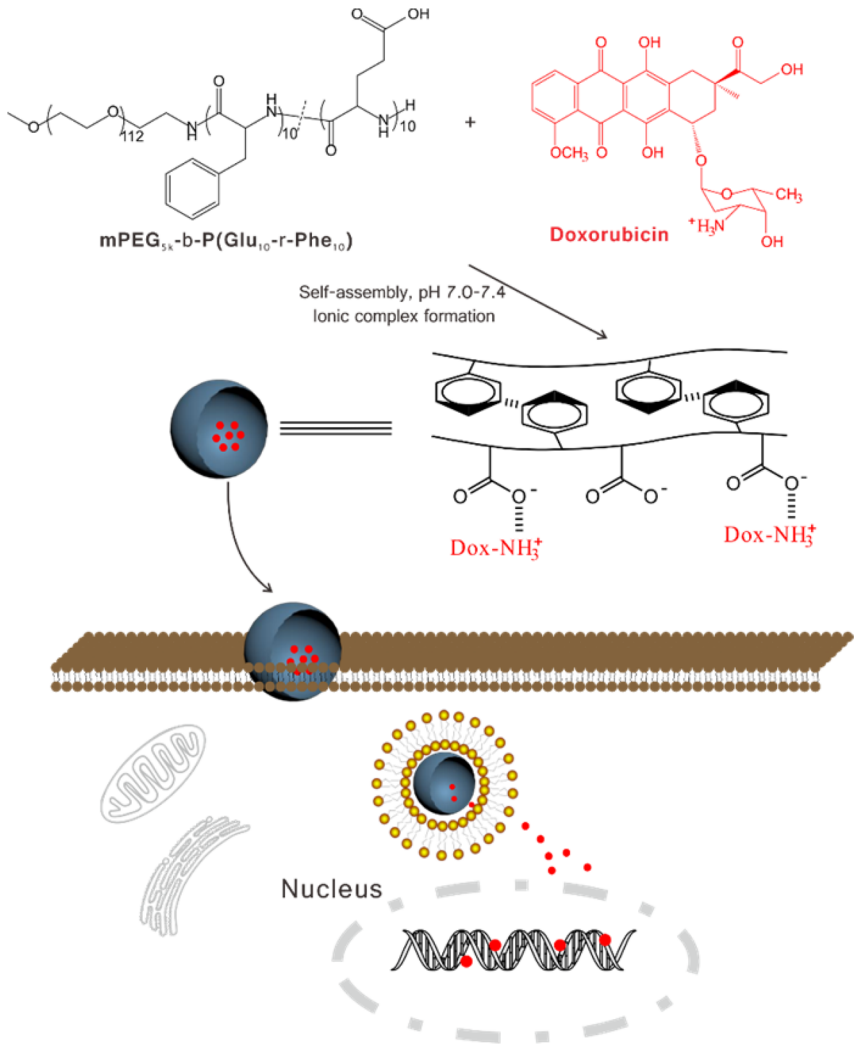

Figure 1. Schematic illustration of the preparation and interaction mechanism of n-Dox.

genetic characters, such as mutated p53,[9] aberrant protein kinase C (PKC),[10] NFκB,[11] and caveolin,[12] except for the P-gP upregulated signaling pathway. Thus, the other signaling pathways could be utilized to regulate the therapeutic sensitivity of resistant cells.

In this work, the therapeutic efficacy of poly(amino acid)−doxorubicin on doxorubicin-resistant tumors was studied. While the cell viability and cell uptake results did not reflect the nanodrug's advantage in resistant tumors, comparison of the genetic expression of sensitive and resistant cells highlighted NFκB. When the proteasome inhibitor bortezomib was employed, the MTT assay and flow cytometry indicated that it could increase the therapeutic efficacy of poly(amino acid)−doxorubicin, and Western blot results showed that bortezomib and poly(amino acid)−doxorubicin can synergistically diminish NFκB expression. The synergism was confirmed through an orthotopic xenograft model in vivo. Thus, bortezomib can enhance the cancer therapeutic efficiency of poly(amino acid)−doxorubicin not only during the sensitive period but also during the resistant period.

MATERIALS AND METHODS

Materials. Doxorubicin·HCl was purchased from Sinopharm Chemical Reagent Co. Ltd. (Beijing, P. R. China). Bortezomib (Bor) was obtained from Beijing HuaFeng United Technology Co., Ltd. (Beijing, P. R. China). Cell culture products, including Rosewell Park Memorial Institute (RPMI) 1640 medium and fetal bovine serum (FBS) were provided by Gibco (Grand Island, NY, USA). Penicillin and streptomycin were obtained from Huabei Pharmaceutical Co., Ltd. (Shijiazhuang, P. R. China). The BCA Protein Assay Kit was purchased from Thermo Pierce Biotechnology (Rockford, IL, USA). 3-(4,5-Dimethylthiazol-2-yl)-2,5-diphenyltetrazolium bromide (MTT) was purchased from Sigma-Aldrich (Shanghai, P. R. China).

Synthesis and Characterizations. Synthesis and characterization of nanoized doxorubicin were performed as reported previously.[4] The molar composition ratio of the monomeric repeating units in $mPEG_{5k}$-*b*-$P(Glu_{10}$-*r*-$Phe_{10})$ was 113:10:10. The number-average molecular weight of $mPEG_{5k}$-*b*-$P(Glu_{10}$-*r*-$Phe_{10})$ calculated by ^1H NMR spectroscopy was 7760 g·mol^{-1}. Gel-permeation chromatography (GPC) analyses showed that the $mPEG_{5k}$-*b*-$P(Glu_{10}$-*r*-$Phe_{10})$ copolymer had a narrow molecular weight distribution (polydispersity index = 1.1). The diameter was 140 nm, and its drug loading content was 19.1%.

Cell Culture. The human breast cancer cell line MCF-7 and its drug-resistant variant MCF-7/Adr were purchased from Shanghai Bogoo Biotechnology Co. Ltd. They were cultured in complete RPMI 1640 medium supplemented with 10% FBS, 100 units·mL^{-1} penicillin, and 100 μg·mL^{-1} streptomycin in a humidified incubator with 5% CO_2 at 37 °C. Before drug treatment, cells were cultured at a density of around 0.3 × 10^6 mL^{-1} overnight to reach 70% confluency.

Cellular Uptake Study. The cellular uptake of Dox and n-Dox was assessed by confocal laser scanning microscopy (CLSM) and fluorescence-activated cell sorting (FACS) against MCF-7 and

DOI: 10.1021/acsbiomaterials.7b00639
ACS Biomater. Sci. Eng. 2018, 4, 2053−2060

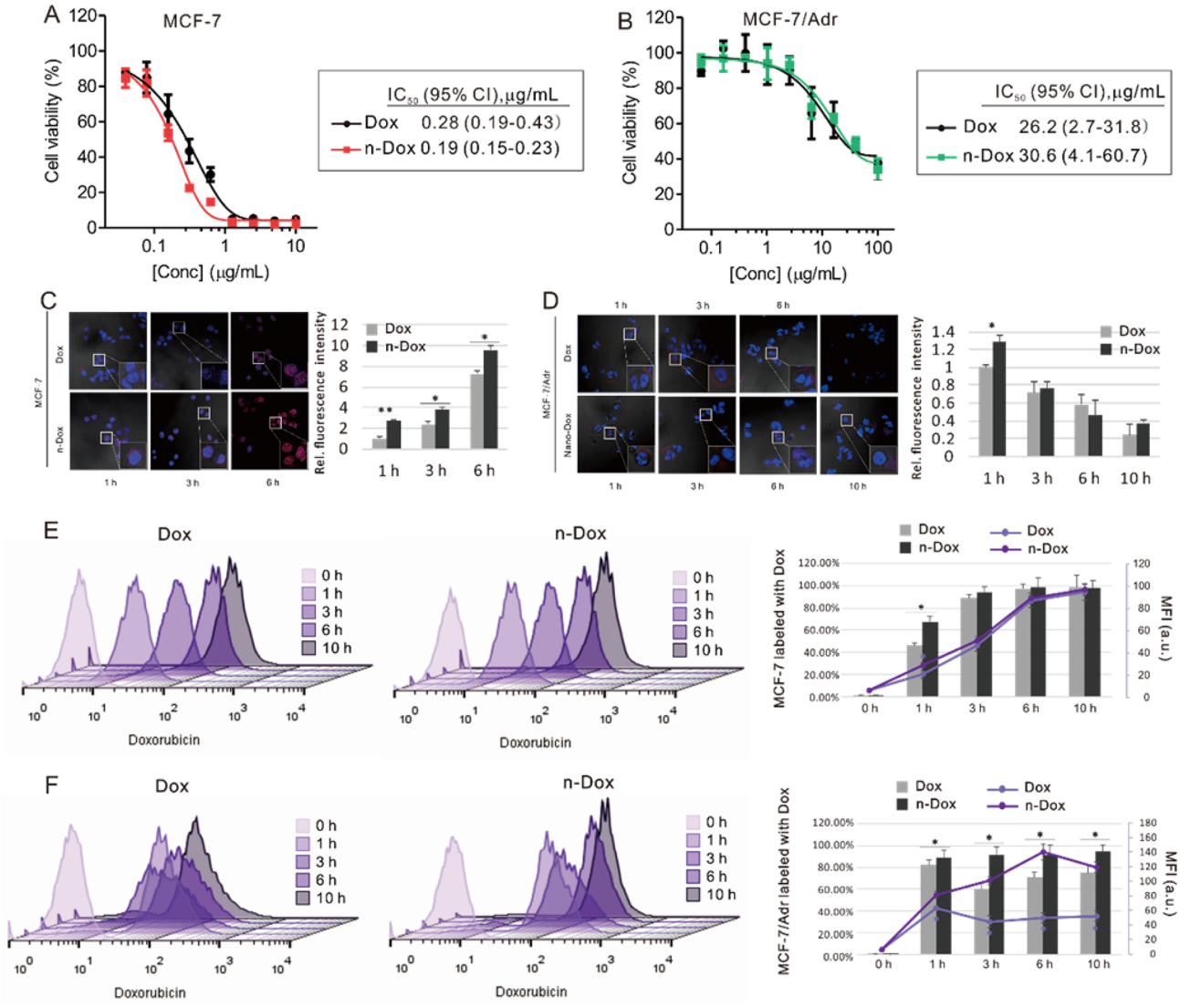

Figure 2. Cytotoxicity and cell uptake of Dox and n-Dox in MCF-7 and MCF-7/Adr cells. (A, B) MTT assay results showing the relative cell viabilities and IC_{50} values in (A) MCF-7 and (B) MCF-7/Adr cells. (C, D) Confocal laser scanning microscopy images (left) and quantification of relative fluorescence intensities (right) of (C) MCF-7 and (D) MCF-7/Adr cells. In the merged pictures, red represents doxorubicin and blue represents DAPI. (E, F) Fluorescence-activated cell sorting data for (E) MCF-7 and (F) MCF-7/Adr cells upon Dox and n-Dox treatment at different times. The relative fluorescence intensities of Dox from all images were analyzed using ImageJ software. Data were reported as mean ± SD from three independent experiments. *, $P < 0.05$ and **, $P < 0.01$ compared with the control as determined by Student's t test.

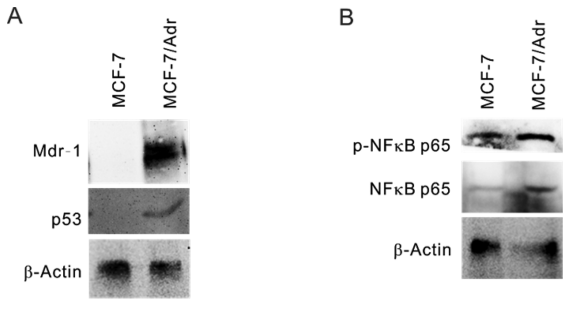

Figure 3. Gene expression differences between MCF-7 and MCF-7/Adr cells. (A) Western blot showing Mdr-1 and p53 expression. (B) Western blot indicating the NFκB p65 and its phosporylation.

MCF-7/Adr cells. The cells were seeded in six-well plates at (2–3) × 10^5 cells per well, precultured in 2.0 mL of complete culture medium overnight, and then incubated for another 1, 3, or 6 h with Dox or n-Dox at 37 °C. For CLSM, cells were washed with phosphate-buffered saline (PBS) (0.01 M, pH 7.4) three times (5 min per wash). Then the cells were fixed with 4% (w/v) paraformaldehyde for 25 min at 25 °C and washed five times with PBS, and the cell nuclei were stained with 4,6-diamidino-2-phenylindole (DAPI) according to the standard protocols from the supplier. CLSM images were taken using a laser scanning confocal microscope (Zeiss). For FACS, cells were collected and washed with PBS (0.01 M, pH 7.4) three times, sorted, and analyzed by flow cytometry. Data were analyzed using FlowJo software.

In Vitro Cytotoxicity Assay. The cytotoxicities of Dox, n-Dox, Bor, and n-Dox and Bor combined were studied using the MTT assay. MCF-7 or MCF-7/Adr cells were seeded in 96-well plates at 7000 cells per well in RPMI 1640 containing 10% FBS overnight. The culture medium was replaced with fresh medium containing drugs at various concentrations for another 24 or 48 h incubation. Then the medium in each well was replaced with 180 μL of fresh medium and 20 μL of MTT (5 mg·mL^{-1} in PBS), and the cells were incubated for another 4 h at 37 °C. The MTT solution was removed and 150 μL of dimethyl sulfoxide (DMSO) was added to each well to dissolve formazan crystals. The absorbance was measured at 490 nm on a Biotek microplate reader. The relative cell viabilities were calculated as $(A_{sample}/A_{control}) \times 100$,

DOI: 10.1021/acsbiomaterials.7b00639
ACS Biomater. Sci. Eng. 2018, 4, 2053–2060

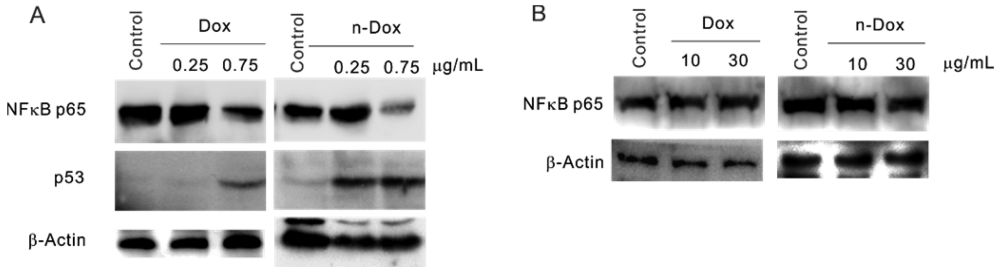

Figure 4. Influence of Dox and n-Dox on NFκB p65 expression. (A) Western blot showing the indicated protein expression after Dox and n-Dox treatment in MCF-7 cells. (B) Western blot for NFκB detection upon Dox and n-Dox treatment in MCF-7/Adr cells.

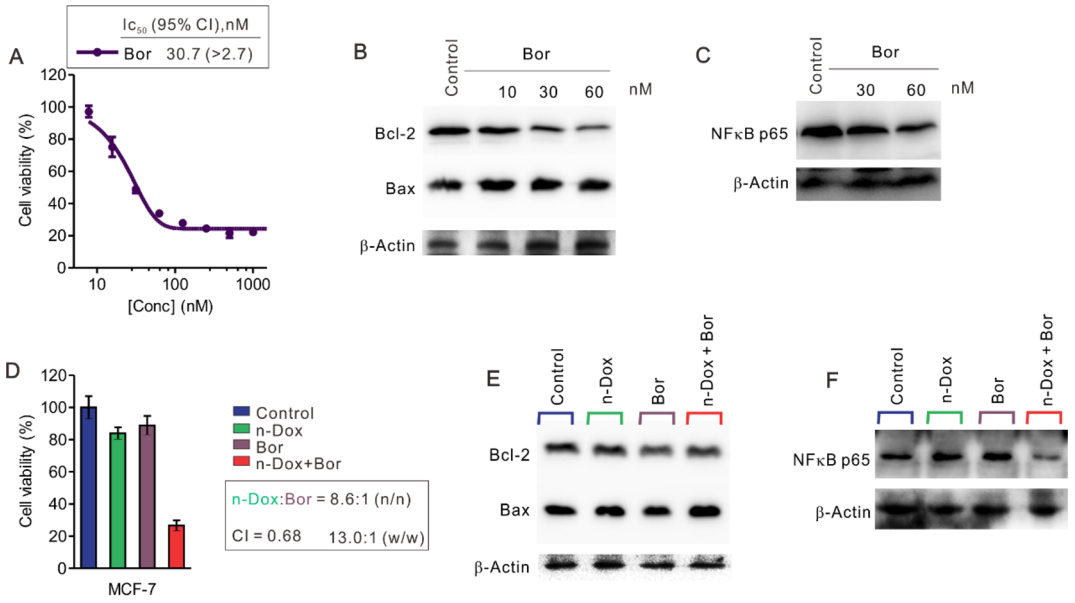

Figure 5. Borteomib is synergistic with n-Dox in doxorubicin-sensitive MCF-7 cells. (A) MTT assay reflecting the cytotoxicity of MCF-7 with different doses of bortezomib. (B) MCF-7 cells were treated with bortezomib for 48 h, and then the protein samples were subjected to Western blot. Apoptotic gene expression was detected. (C) Western blot showing NFκB expression in bortezomib-treated MCF-7 cells. (D) MTT assay demonstrating the cell viability change after n-Dox or/and bortezomib treatment. (E, F) MCF-7 cells were treated with n-Dox or/and bortezomib for 48 h, and the protein samples were then subjected to Western blot. The indicated apoptosis-related gene (E) and NFκB expression (F) were investigated.

where A_{sample} and $A_{control}$ are the absorbances of the sample well and control well, respectively. Data were presented as mean ± standard deviation (SD) (n = 3). The data were analyzed with Graphpad Prism software. The points were fitted by nonlinear regression, and the half-maximal inhibitory concentrations (IC_{50}) were obtained according to the log(inhibition)−response curve.

Quantitative Determination of Drug Interactions. Drug interactions were evaluated through combination index (CI) analysis based on the Chou−Talay method[13] and the following equation:

$$CI = D_1/D_{x1} + D_2/D_{x2}$$

where D_1 and D_2 represent the concentrations of drug 1 and drug 2 that in combination give the same response as drug 1 alone (D_{x1}) or drug 2 alone (D_{x2}). CI values less than, equal to, and greater than 1 indicate synergism, additive effect, and antagonism, respectively.

Cell Apoptosis Study. Propidium iodide (PI) (Sigma-Aldrich) or 7-aminoactinomycin D (7-AAD) uptake was taken as a measure of cell membrane permeability, and annexin V−FITC binding was used as a measure of cell membrane scrambling with phosphatidylserine translocation at the cell surface, as described previously[14,15]. To this end, the drug-treated cells were incubated with annexin V−FITC and PI (MCF-7) or annexin V−FITC and 7-AAD (MCF-7/Adr) to assess cell apoptosis and necrosis. The labeled samples were then determined by flow cytometry using a FACSCalibur flow cytometer (BD Biosciences, Heidelberg, Germany).

Western Blot. Western blotting was carried out with whole-cell lysates as previously described.[16] As to single treatment, MCF-7 cells were treated with 0.25 or 0.75 $\mu g \cdot mL^{-1}$ Dox or n-Dox or 10, 30, or 60 nM Bor for 48 h, while MCF-7/Adr cells were treated with 10 or 30 $\mu g \cdot mL^{-1}$ Dox or n-Dox or 1, 2, or 5 μM Bor for 48 h. For combination treatment, MCF-7 cells were treated with 0.15 $\mu g \cdot mL^{-1}$ n-Dox and 30 nM Bor for 48 h, and MCF-7/Adr cells were treated with 10 $\mu g \cdot mL^{-1}$ n-Dox and 2 μM Bor for 48 h. Whole-cell proteins were prepared by lysing the cells in 1× cell lysis buffer [2 mM Tris-HCl (pH 7.5), 15 mM NaCl, 0.1% Triton] supplemented with proteinase inhibitors. After protein lysates were quantified, 10−40 μg of protein was loaded into 6% or 15% polyacrylamide SDS-PAGE gels and transferred to PVDF membranes (Millipore). β-Actin was used as an internal reference. Antibodies used were as follows: NFκB p65, Bcl-2, and Bax from Abcam; Mdr-1 and β-actin from Santa Cruz; and p-NFκB p65 from Cell Signaling. The proteins detected were visualized using an enhanced chemiluminescence Western blot detection system (Tanon Science & Technology Co. Ltd.).

In Vivo Tumorigenicity Assays. Nude mice (female, 6 weeks old) were purchased from Beijing Vital River Laboratory Animal Technology Co., Ltd. All of the animal experiments were performed in accordance with the Guide for Care and Use of Laboratory Animals and were approved by the Animal Care and Use Committee of Jilin University. To build the MCF-7 orthotopic xenograft model, about 2 × 10^6 MCF-7 cells were injected subcutaneously into the right

DOI: 10.1021/acsbiomaterials.7b00639
ACS Biomater. Sci. Eng. 2018, 4, 2053−2060

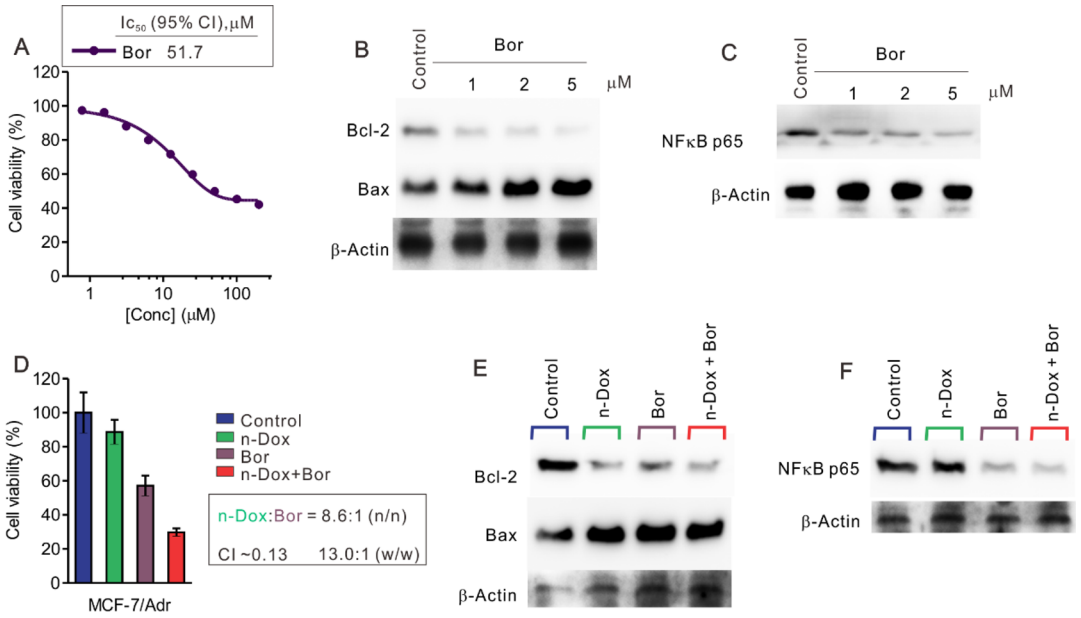

Figure 6. Borteomib is synergistic with n-Dox in doxorubicin-resistant MCF-7/Adr cells. (A) MTT assay reflecting the cytotoxicity of MCF-7/Adr with different doses of bortezomib. (B) MCF-7/Adr cells were treated with bortezomib for 48 h, and then the protein samples were subjected to Western blot. Apoptotic gene expression was detected. (C) Western blot showing NFκB expression in bortezomib-treated MCF-7/Adr cells. (D) MTT assay demonstrating the cell viability change after n-Dox or/and bortezomib treatment. (E, F) MCF-7/Adr cells were treated with n-Dox or/and bortezomib for 48 h, and the protein samples were then subjected to Western blot. The indicated apoptosis-related gene (E) and NFκB expression (F) were tested.

mammary fat pad of each mouse for xenograft tumor (n = 6 mice per group). When the tumor volume was approximately 50 mm^3, the mice were divided into four groups and then treated with PBS, n-Dox (1.5 $mg{\cdot}kg^{-1}$ on a Dox·HCl basis), Bor (0.115 $mg{\cdot}kg^{-1}$), or n-Dox plus Bor (1.5 $mg{\cdot}kg^{-1}$ on a Dox·HCl basis, 0.115 $mg{\cdot}kg^{-1}$) by tail intravenous injection on days 1, 4, 8, and 11. To build the MCF-7/Adr orthotopic xenograft model, about 10×10^6 MCF-7/Adr cells (resuspended in 1:1 PBS:Matrigel) were injected subcutaneously into the right mammary fat pad of each mouse for xenograft tumor (n = 6 mice per group). When the tumor volume was approximately 50 mm^3, the mice were divided into four groups and then treated with PBS, n-Dox (2.5 $mg{\cdot}kg^{-1}$ on a Dox·HCl basis), Bor (0.192 $mg{\cdot}kg^{-1}$), or n-Dox plus Bor (2.5 $mg{\cdot}kg^{-1}$ on a Dox·HCl basis, 0.192 $mg{\cdot}kg^{-1}$) by tail intravenous injection on days 1, 4, 8, and 11. The tumor sizes were measured every 2 days. The tumor volume (in mm^3) was calculated using $V = ab^2/2$,[17] where a and b stand for the longest and shortest diameters of the tumor, respectively. All of the tumors were excised at the same time. The liver, spleen, lung, and kidney sections were collected and together with the tumors were fixed in 4% paraformaldehyde.

Hematoxylin and Eosin (H&E) Staining. Tumors and tissues collected from our animal studies were fixed with 4% paraformaldehyde. The paraffin-embedded samples were cut to 5 μm thickness and stained with H&E.

Statistical Analysis. The quantification was analyzed using Student's t test. All of the statistical analyses were conducted using GraphPad Prism 5.0 (GraphPad Software, Inc., La Jolla, CA, USA). Differences were considered statistically significant at $P < 0.05$. All of the P values were two-sided.

RESULTS AND DISCUSSION

Comparison of Cytotoxicity and Endocytosis between n-Dox and Dox. The structure, composition, and function of poly(amino acid)−Dox are shown in Figure 1. Doxorubicin-sensitive MCF-7 and doxorubicin-resistant MCF-7/Adr cells were employed in this study. On the basis of the study of MCF-7, n-Dox indeed exhibited stronger cytotoxicity, with IC_{50} values of 0.28 $\mu g{\cdot}mL^{-1}$ for Dox and 0.19 $\mu g{\cdot}mL^{-1}$ for n-Dox (Figure 2A). The FACS and CLSM results showed faster and greater uptake of n-Dox compared with Dox, and the drug was concentrated in the nuclei of cells (Figure 2C,E). The fluorescence intensity was obviously higher at 1, 3, and 6 h, and the counted number of labeled cells at 1 h was greater for n-Dox treatment.

However, when MCF-7/Adr cells were treated with Dox and n-Dox, the drug concentration had to be increased greatly to obtain cytotoxicity. The IC_{50} values were 26.2 $\mu g{\cdot}mL^{-1}$ (Dox) and 30.6 $\mu g{\cdot}mL^{-1}$ (n-Dox) ($P > 0.05$). This seems to indicate that poly(amino acid)−doxorubicin did not excel compared with free doxorubicin in regard to toxicity (Figure 2B). To this end, the cell uptake was evaluated through CLSM and FACS (Figure 2D,F). The fluorescence intensity was obviously higher at 1 h, and the counted numbers of labeled cells at 1, 3, 6, and 10 h were greater for n-Dox treatment. Endocytosis of n-Dox was faster and greater than that of free doxorubicin, and the location of drug after uptake was mainly concentrated in cell plasma. Therefore, it is the drug location, further the drug release, that may limit the therapeutic efficacy of poly(amino acid)−doxorubicin in MCF-7/Adr cells.

Gene Expression Difference between Doxorubicin-Sensitive and -Resistant Cells. Since the poly(amino acid)−doxorubicin had an advantage in treating doxorubicin-sensitive cells but not doxorubicin-resistant cells, we wondered what is the genetic mechanism for this. Thus, the gene expression difference between MCF-7 and MCF-7/Adr cells was assessed. It has been reported that multidrug-resistant protein P-gP was highly expressed and the apoptotic-related p53 protein was mutated in resistant cells. This was confirmed through Western blot, and the results showed that Mdr-1 protein was overexpressed and the p53 (mutated p53) protein was expressed strongly in MCF-7/Adr cells compared with MCF-7 cells (Figure 3A). As it showed that NFκB may influence the therapeutic result of multiple myeloma, NFκB p65 and its phosphorylation were explored in the Dox-sensitive and -resistant cells (Figure 3B).

DOI: 10.1021/acsbiomaterials.7b00639
ACS Biomater. Sci. Eng. 2018, 4, 2053−2060

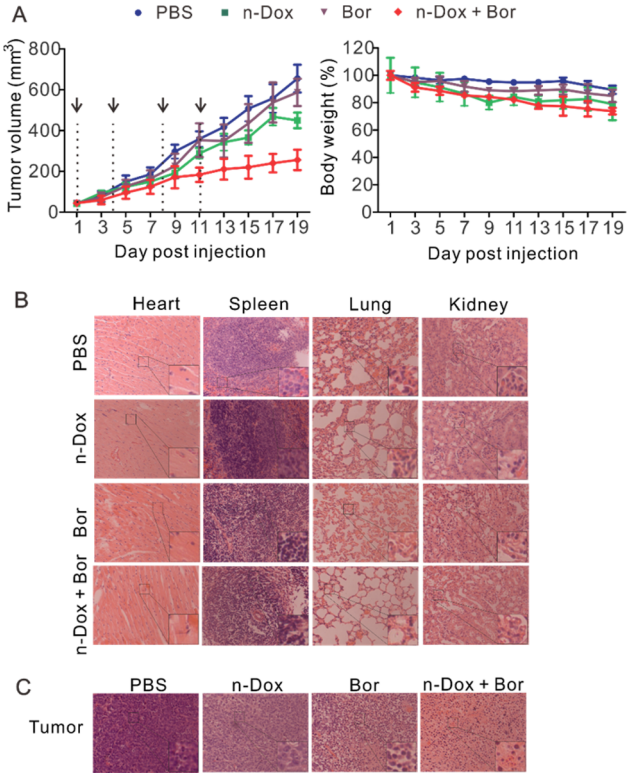

Figure 7. Bortezomib increases n-Dox therapeutic efficacy toward MCF-7 xenografted tumor. About 2×10^6 MCF-7 cells were injected subcutaneously into the right mammary fat pad of each mouse for xenograft tumor (n = 6 mice per group). When the tumor volume was approximately 50 mm^3, the mice were divided into four groups and then treated with PBS, n-Dox (1.5 $mg \cdot kg^{-1}$ on a Dox·HCl basis), bortezomib (0.115 $mg \cdot kg^{-1}$), or n-Dox plus bortezomib (1.5 $mg \cdot kg^{-1}$ on a Dox·HCl basis, 0.115 $mg \cdot kg^{-1}$) by tail intravenous injection on days 1, 4, 8, and 11. (A) Tumor growth curve and body weight change after n-Dox or/and bortezomib treatment. (B) H&E staining for heart, spleen, lung, and kidney after treatment. (C) H&E staining for tumor after treatment (200× magnification).

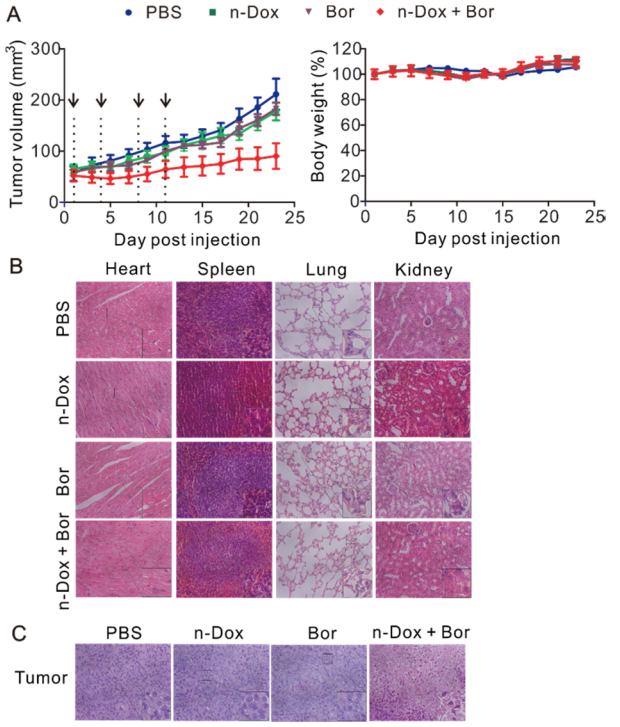

Figure 8. Bortezomib increases n-Dox therapeutic efficacy toward MCF-7/Adr xenografted tumor. About 10×10^6 MCF-7/Adr cells (resuspended in 1:1 PBS:Matrigel) were injected subcutaneously into the right mammary fat pad of each mouse for xenograft tumor (n = 6 mice per group). When the tumor volume was approximately 50 mm^3, the mice were divided into four groups and then treated with PBS, n-Dox (2.5 $mg \cdot kg^{-1}$ on a Dox·HCl basis), bortezomib (0.192 $mg \cdot kg^{-1}$), or n-Dox plus bortezomib (2.5 $mg \cdot kg^{-1}$ on a Dox·HCl basis, 0.192 $mg \cdot kg^{-1}$) by tail intravenous injection on days 1, 4, 8, and 11. (A) Tumor growth curve and body weight change after n-Dox or/and bortezomib treatment. (B) H&E staining for heart, spleen, lung, and kidney after treatment. (C) H&E staining for tumor after treatment (200× magnification).

The results revealed that the oncogenic NFκB p65 exists more and that the elevated phosphorylation influences the function of NFκB. Together, the elevated NFκB may cause the resistant cells became aberrant and tough to kill.

Influence of Dox and n-Dox on NFκB p65 Expression. First, we evaluated the effect of Dox and n-Dox on NFκB expression in both Dox-sensitive and -resistant cells. Western blot experiments were performed, and the results showed that n-Dox could induce diminished NFκB to a greater extent than Dox in MCF-7 cells (Figure 4A). However, the n-Dox did not significantly decrease NFκB expression in MCF-7/Adr cells compared with Dox (Figure 4B). Thus, this revealed that NFκB expression had some accordance with the sensitivity of drug treatment and cell response.

Bortezomib Increases Poly(amino acid)−Doxorubicin Therapeutic Efficacy in Vitro. Bortezomib is a classic proteasome inhibitor, and it has been reported that bortezomib can disrupt SP1 and NFκB association, influence NFκB activity, and regulate leukemia cell fate. Here, bortezomib was applied to diminish the NFκB activity in order to see whether it can enhance doxorubicin nanodrug's therapeutic sensitivity.

The sensitivity of n-Dox treatment in MCF-7 cells was first explored. As shown in Figure 5A−C, bortezomib exhibited cytotoxicity toward MCF-7 cells. The pro-apoptotic gene Bax was upregulated and the anti-apoptotic gene Bcl-2 was downregulated, which indicates that bortezomib can induce cell apoptosis. When n-Dox was combined with bortezomib, the cytotoxcixity was synergistically enhanced compared with the n-Dox or bortezomib single treatment (Figure 5D). The changes in apoptotic-related gene expression revealed that n-Dox and bortezomib can induce apoptosis (Figure 5E). From the mechanism, they can synergistically decrease NFκB expression (Figure 5F).

The synergism of n-Dox and bortezomib triggered us to apply the regimen to doxorubicin-resistant MCF-7/Adr cells. As shown in Figure 6A−C, bortezomib exhibited cytotoxicity toward MCF-7/Adr cells. The pro-apoptotic gene Bax was upregulated, and the anti-apoptotic gene Bcl-2 was downregulated. This indicates that bortezomib can induce cell apoptosis. When n-Dox was combined with bortezomib, the cytotoxicity was synergistically enhanced compared with the n-Dox or bortezomib single treatment (Figure 6D). The changes in apoptotic-related gene expression revealed that n-Dox and bortezomib can induce apoptosis (Figure 6E). From the mechanism, they can synergistically decrease NFκB expression (Figure 6F).

Bortezomib Increases Poly(amino acid)−Doxorubicin Therapeutic Efficacy in Vivo. Since good results were obtained in vitro, we performed the tumor inhibitory experiments in vivo. An orthotopic xenograft model was established on the basis of the previous report, and nude mice were employed. MCF-7

DOI: 10.1021/acsbiomaterials.7b00639
ACS Biomater. Sci. Eng. 2018, 4, 2053−2060

cells (2×10^6, resuspended in PBS) or MCF-7/Adr cells (10×10^6, resuspended in 1:1 PBS:Matrigel) were injected subcutaneously into the right mammary fat pad of mice. As shown in Figure 7A, n-Dox and bortezomib could synergistically inhibit the MCF-7 tumor growth and give a smaller tumor relative to n-Dox or bortezomib single treatment ($P < 0.05$). From the body weight change image, the combination treatment scheme exhibits little toxicity (Figure 7B). Moreover, histological staining showed that the drug did not have much toxicity toward tissues like heart, spleen, lung, and kidney (Figure 7C). When the tumors were fixed, sliced, and stained with H&E, low- and high-power magnification of H&E staining demonstrated clear apoptosis with typical apoptotic bodies. Diffuse tumor cell growth without signs of apoptosis or necrosis in untreated tumors and confluent areas of necrosis with typical loss of nuclei could be found (Figure 7D). Similar results were obtained in MCF-7/Adr xenograft tumors, as n-Dox and bortezomib could synergistically inhibit the MCF-7/Adr tumor growth ($P < 0.01$) without significant toxicity (Figure 8A,B). Furthermore, the treatment strategy did not have obvious toxicity toward the heart, spleen, lung, and kidney (Figure 8C). The histological staining of tumors showed that n-Dox and bortezomib combination treatment resulted in more apoptosis and necrosis (Figure 8D).

From the above tumor growth inhibition results, the n-Dox and bortezomib combination treatment strategy was more effective in the resistant tumors compared with n-Dox or bortezomib single treatment. Thus, bortezomib could increase the therapeutic efficacy of n-Dox toward both doxorubicin-sensitive and -resistant tumors. Therefore, bortezomib may prolong the application time of the poly(amino acid)−doxorubicin nanodrug not only at the initiation of treatment but also even when the tumor becomes resistant to the doxorubicin. To this end, bortezomib can make the poly(amino acid)−doxorubicin a "universal" drug. This makes bortezomib and poly(amino acid)−doxorubicin a potential combination program in the clinic, and poly(amino acid)−doxorubicin could be a clinical anticancer drug candidate.

CONCLUSION

This work studied the effect of poly(amino acid)−doxorubicin nanodrug on doxorubicin-sensitive MCF-7 cells and doxorubicin-resistant MCF-7/Adr cells. It highlighted that NFκB overexpression may limit the poly(amino acid)−doxorubicin therapeutic sensitivity in MCF-7/Adr cells. The proteasome inhibitor bortezomib was employed to diminish the NFκB activity, which indeed increased the therapeutic efficacy of poly(amino acid)−doxorubicin. Thus, bortezomib could enhance the cancer therapeutic efficiency of poly(amino acid)−doxorubicin not only during the sensitive period but also during the resistant period. This makes the bortezomib and poly(amino acid)−doxorubicin combination a potent strategy and guidance for the clinic.

AUTHOR INFORMATION

Corresponding Author

*E-mail: ztang@ciac.ac.cn.

ORCID

Na Shen: 0000-0003-1557-1060

Xuesi Chen: 0000-0003-3542-9256

Notes

The authors declare no competing financial interest.

ACKNOWLEDGMENTS

The studies reported here were financially supported by National Natural Science Foundation of China (Projects 51673189 and 51503202) and the Chinese Academy of Sciences Youth Innovation Promotion Association.

ABBREVIATIONS

Dox, doxorubicin; n-Dox, nanoized doxorubicin, poly(amino acid)−doxorubicin; Bor, bortezomib; IC_{50}, half-maximal inhibitory concentration; IF, immunofluorescence; MTT, 3-(4,5-dimethyl-2-thiazolyl)-2,5-diphenyl-2*H*-tetrazolium bromide; CLSM, confocal laser scanning microscopy; FACS, fluorescence-activated cell sorting

REFERENCES

(1) Wu, L.; Xu, J.; Yuan, W.; Wu, B.; Wang, H.; Liu, G.; Wang, X.; Du, J.; Cai, S. The reversal effects of 3-bromopyruvate on multidrug resistance in vitro and in vivo derived from human breast MCF-7/ADR cells. *PLoS One* **2014**, *9* (11), e112132.

(2) Nam, K.; Nam, H. Y.; Kim, P. H.; Kim, S. W. Paclitaxel-conjugated PEG and arginine-grafted bioreducible poly (disulfide amine) micelles for co-delivery of drug and gene. *Biomaterials* **2012**, *33* (32), 8122−30.

(3) Mu, L. M.; Ju, R. J.; Liu, R.; Bu, Y. Z.; Zhang, J. Y.; Li, X. Q.; Zeng, F.; Lu, W. L. Dual-functional drug liposomes in treatment of resistant cancers. *Adv. Drug Delivery Rev.* **2017**, *115*, 46−56.

(4) Lv, S. X.; Li, M. Q.; Tang, Z. H.; Song, W. T.; Sun, H.; Liu, H. Y.; Chen, X. S. Doxorubicin-loaded amphiphilic polypeptide-based nanoparticles as an efficient drug delivery system for cancer therapy. *Acta Biomater.* **2013**, *9* (12), 9330−9342.

(5) Wu, Q.; Yang, Z. P.; Nie, Y. Z.; Shi, Y. Q.; Fan, D. M. Multi-drug resistance in cancer chemotherapeutics: Mechanisms and lab approaches. *Cancer Lett.* **2014**, *347* (2), 159−166.

(6) Wu, H.; Hait, W. N.; Yang, J. M. Small interfering RNA-induced suppression of MDR1 (P-glycoprotein) restores sensitivity to multidrug-resistant cancer cells. *Cancer Res.* **2003**, *63* (7), 1515−1519.

(7) Ju, R. J.; Mu, L. M.; Lu, W. L. Targeting drug delivery systems for circumventing multidrug resistance of cancers. *Ther. Delivery* **2013**, *4* (6), 667−71.

(8) Feng, Q.; Liu, J.; Li, X.; Chen, Q.; Sun, J.; Shi, X.; Ding, B.; Yu, H.; Li, Y.; Jiang, X. One-Step Microfluidic Synthesis of Nanocomplex with Tunable Rigidity and Acid-Switchable Surface Charge for Overcoming Drug Resistance. *Small* **2017**, *13* (9), 201603109.

(9) Aas, T.; Borresen, A. L.; Geisler, S.; Smith-Sorensen, B.; Johnsen, H.; Varhaug, J. E.; Akslen, L. A.; Lonning, P. E. Specific P53 mutations are associated with de novo resistance to doxorubicin in breast cancer patients. *Nat. Med.* **1996**, *2* (7), 811−4.

(10) Tsuruo, T.; Naito, M.; Tomida, A.; Fujita, N.; Mashima, T.; Sakamoto, H.; Haga, N. Molecular targeting therapy of cancer: drug resistance, apoptosis and survival signal. *Cancer Sci.* **2003**, *94* (1), 15−21.

(11) Mitsiades, N.; Mitsiades, C. S.; Richardson, P. G.; Poulaki, V.; Tai, Y. T.; Chauhan, D.; Fanourakis, G.; Gu, X.; Bailey, C.; Joseph, M.; Libermann, T. A.; Schlossman, R.; Munshi, N. C.; Hideshima, T.; Anderson, K. C. The proteasome inhibitor PS-341 potentiates sensitivity of multiple myeloma cells to conventional chemotherapeutic agents: therapeutic applications. *Blood* **2003**, *101* (6), 2377−2380.

(12) Yang, C. P.; Galbiati, F.; Volonte, D.; Horwitz, S. B.; Lisanti, M. P. Upregulation of caveolin-1 and caveolae organelles in Taxol-resistant A549 cells. *FEBS Lett.* **1998**, *439* (3), 368−72.

(13) Chou, T. C. Theoretical basis, experimental design, and computerized simulation of synergism and antagonism in drug combination studies. *Pharmacol Rev.* **2006**, *58* (3), 621−681.

(14) Zeng, N.; Zhou, Y.; Zhang, S.; Singh, Y.; Shi, B.; Salker, M. S.; Lang, F. 1alpha,25(OH) 2D3 Sensitive Cytosolic pH Regulation and Glycolytic Flux in Human Endometrial Ishikawa Cells. *Cell. Physiol. Biochem.* **2017**, *41* (2), 678−688.

DOI: 10.1021/acsbiomaterials.7b00639
ACS Biomater. Sci. Eng. 2018, 4, 2053−2060

(15) Towhid, S. T.; Liu, G. L.; Ackermann, T. F.; Beier, N.; Scholz, W.; Fuchss, T.; Toulany, M.; Rodemann, H. P.; Lang, F. Inhibition of colonic tumor growth by the selective SGK inhibitor EMD638683. *Cell. Physiol. Biochem.* **2013**, *32* (4), 838−48.
(16) Shen, N.; Yan, F.; Pang, J.; Zhao, N.; Gangat, N.; Wu, L.; Bode, A. M.; Al-Kali, A.; Litzow, M. R.; Liu, S. Inactivation of Receptor Tyrosine Kinases Reverts Aberrant DNA Methylation in Acute Myeloid Leukemia. *Clin. Cancer Res.* **2017**, *23* (20), 6254−6266.
(17) Nie, F. Q.; Yu, X.; Huang, M. D.; Wang, Y. F.; Xie, M.; Ma, H. W.; Wang, Z. X.; De, W.; Sun, M. Long noncoding RNA ZFAS1 promotes gastric cancer cells proliferation by epigenetically repressing KLF2 and NKD2 expression. *Oncotarget* **2017**, *8* (24), 38227−38238.

DOI: 10.1021/acsbiomaterials.7b00639
ACS Biomater. Sci. Eng. 2018, 4, 2053−2060